Well-Defined Ti Surface Sites in Ziegler-Natta Pre-Catalysts from $^{47/49}$Ti Solid-State Nuclear Magnetic Resonance Spectroscopy

Alexander V. Yakimov[a,‡,*], Christoph J. Kaul[a,‡], Yuya Kakiuchi[a], Sebastian Sabisch[a], Felipe Morais Bolner[b], Jean Raynaud[b], Vincent Monteil[b], Pierrick Berruyer[c], Christophe Copéret[a,*]

[a] Department of Chemistry and Applied Biosciences, Laboratory of Inorganic Chemistry, Surface & Interfacial Chemistry, Eidgenössische Technische Hochschule Zürich, HCI, Vladimir-Prelog-Weg 2, CH-8093 Zurich, Switzerland

[b] Université de Lyon, CNRS, Université Lyon 1, CPE Lyon, UMR 5128 - CP2M (Catalysis, Polymerization, Processes & Materials), PolyCatMat team, 69616 Villeurbanne, France

[c] Institut des Sciences et Ingenierie Chimiques, École Polytechnique Fedérale de Lausanne (EPFL), CH-1015, Lausanne, Switzerland

KEYWORDS. Ziegler-Natta catalysts, solid-state NMR, DFT calculations, High-field $^{47/49}$Ti NMR.

ABSTRACT: Treatment of Ziegler-Natta (ZN) catalysts with BCl_3 improves their activity by increasing the number of active sites. Here we show how $^{47/49}$Ti solid-state nuclear magnetic resonance (NMR) spectroscopy enables to understand the electronic structure of the Ti surface sites present in such ZN pre-catalysts, prior to activation with alkyl aluminium. High-field (21.1 T) and low temperature (~100 K) NMR augmented by DFT modelling on the pre-catalyst and corresponding molecular analogues enables the detection of $^{47/49}$Ti NMR signatures and a molecular level understanding of the electronic structure of Ti surface sites. The associate Ti surface sites exhibit ^{49}Ti NMR signatures ($\delta_{iso,\,exp}$ = –170 ppm / $C_{Q,\,exp}$ = 9.3 MHz / κ = 0.05) corresponding to well-defined fully chlorinated hexacoordinated Ti sites adsorbed on a distorted surface of the $MgCl_2$ support, formed upon post-treatment with BCl_3 and removal of the alkoxo ligands, paralleling with the increased polymerization activity.

TOC Graphic:

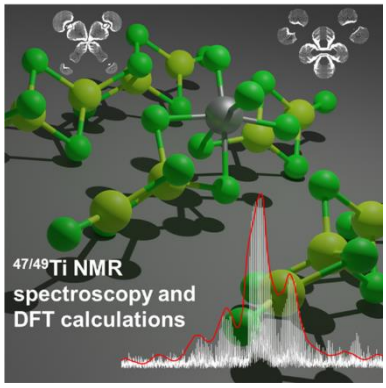

Heterogeneous Ziegler-Natta (ZN) catalysts[1-3] are central for the industrial production of polyethylene (PE grades such as HDPE & LLDPE) and polypropylene (PP such as *iso*PP).[4] These catalysts are multicomponent hybrid materials that include organic (ether, alcohol and esters, referred to as internal donors) and inorganic components ($TiCl_4/MgCl_2$),[5] which trigger polymerization upon activation with alkyl aluminum, *e.g.* triethylaluminum (TEA, $Al(C_2H_5)_3$). The presence of additional organic promoters (external donors) can help to provide polymers with specific properties resulting from the molar masses, the dispersity and the stereoselectivity when applicable (*iso*PP).[6] Despite intensive studies over the past decades,[7-16] establishing structure–activity relationships in ZN catalysts has remained challenging. The situation is particularly challenging because of the low Ti weight loading (2-4 wt. %), and the multistep catalyst preparation, where the state of Ti sites and the structure of the $MgCl_2$ support undergoes changes at every stage. This process ultimately results in a small fraction of catalytically active Ti sites upon activation with alkyl aluminum reagents.[17]

Electron paramagnetic resonance (EPR) spectroscopy combined with DFT modeling has recently enabled identification of the spectroscopic signature of active Ti sites in activated ZN PE catalysts and their attribution to a specific structural motif, namely a bimetallic Ti(III)/Al alkyl species.[17] Despite these advances, establishing a link between the Ti site structures before and after activation remains an important question in order to establish the role of $MgCl_2$ on the structure of the surface sites and detailed structure-activity relationships. The preparation protocol of $MgCl_2$ is known to be critical to generate highly active catalysts,[18] and understanding the interaction of Ti with the support surface is further complicated by the loss of crystallinity

of $MgCl_2$ upon interaction with $TiCl_4$.[19] Thus, structural investigations based on XRD or other techniques that rely on long-range order, are limited. While optical spectroscopy (IR, UV-Vis, Raman)[14], XAS techniques[20] and various multinuclear NMR (^1H, ^{13}C, ^{25}Mg, and ^{35}Cl)[21-25] methods have been used to address the structure of Ti sites on $MgCl_2$, the results have been difficult to interpret and lead to rather poor molecular-level understanding. Furthermore, previous studies have also shown that the internal donors such as THF or ethanol, that are known to help activating $MgCl_2$, are non-innocent and react with $TiCl_4$, thus forming surface Ti alkoxo species,[26, 27] that can explain the broad range of reactivity of surface sites. In fact, the addition of BCl_3 (and other MCl_x additives) has been proposed to remove surface alkoxo species *via* transmetallation by forming B-alkoxo species. Notably this treatment also results in a significant removal of Ti sites (see Table S2 for elemental analysis) and increases the number of active sites upon activation with TEA.[17, 26-28]

Thus, resolving the structure of Ti surface sites formed upon adsorption of $TiCl_4$ on activated $MgCl_2$ is still of prime interest and calls for the development of characterization techniques that can probe the local environment and electronic structure of the Ti sites. Considering that these sites are Ti(IV) and diamagnetic, $^{47/49}$Ti NMR appears to be a suitable candidate. However, $^{47/49}$Ti NMR spectroscopy suffers from a number of critical limitations, namely i) the low gyromagnetic ratio of both ^{49}Ti and ^{47}Ti nuclei, ii) the low natural abundance of these nuclei (5.41 and 7.44 %), iii) the quadrupolar nature of the nuclei (I = 7/2 and 5/2), iv) the rather large quadrupole moment of both nuclei (24.7 and 30.2 fm^2),[29] and v) the close proximity of the isotropic chemical shifts (δ_{iso}) of these isotopes in the NMR spectra (within 267 ppm), often yielding overlapping broad lines.[30] All these factors contribute to the difficulty in obtaining high quality $^{47/49}$Ti NMR spectra, usually associated with a poor signal-to-noise ratio and complex line shapes. The situation is further worsened for ZN pre-catalysts due to the low amount of Ti (often 2-4 wt. %), the expected heterogeneity of surface sites formed upon the adsorption of $TiCl_4$ on specific sites of $MgCl_2$ (*e.g.* the presence of Ti with both Cl and OR ligands).[26, 27] Pioneering work on $^{47/49}$Ti NMR of ZN pre-catalysts led to observation of a very broad low-intense signal, which is difficult to interpret.[31-33] However, recent hardware developments (higher fields, low temperature) augmented with computational approaches have shown that it is possible to detect the NMR signature of Ti sites in Ti silicalite (TS-1), another industrially relevant materials containing only 1-2 wt% Ti.[34]

A specific challenge associated with the characterization of the ZN catalyst is $MgCl_2$ itself. Its disordered character (upon adsorption of $TiCl_4$)[19] makes the development of meaningful DFT models particularly challenging, due to the lack of the corresponding crystal structure. Consequently, previously Ti surface models used for DFT computations were based on $TiCl_4$ adsorbed on various facets of crystalline $MgCl_2$.[31] However, recent findings related to the characterization of the corresponding V-based ZN pre-catalysts (prepared by adsorption of $VOCl_3$ on similar $MgCl_2$) have shed light on how the morphology of $MgCl_2$ can affect the structure and signature of the V sites, thanks to the high sensitivity of ^{51}V NMR combined with computations.[35] Namely, adsorption of $VOCl_3$ on $MgCl_2$-$(THF)_{1.5}$ generates a well-defined V-alkoxo surface species, with a distorted local geometry due to loss of crystallinity of $MgCl_2$.[35]

Encouraged by the advances in solid-state NMR and computational modeling, along with our improved understanding of $MgCl_2$ and its impact on the local geometry of surface sites, we investigate here the corresponding Ti-based ZN PE pre-catalysts by combining high magnetic field (21.1 T), magic angle spinning (MAS), low temperature (~100 K), higher filling factor (3.2 mm thin-wall rotor, ~40 µL sample volume), and probe optimized for low-gamma nuclei, with DFT computations benchmarked on molecular compounds. This multipronged approach unveils the structure of Ti sites in ZN PE catalysts, prepared from the adsorption of $TiCl_4$ on $MgCl_2$ followed by a BCl_3 treatment.[28]

We first conducted $^{47/49}$Ti NMR measurements on two molecular complexes to assess the effect on NMR signatures of specific Ti local environments, representative of possible surface sites, namely $[H_2NMe_2]_2[TiCl_6]$[36] and $[H_2NMe_2]_2[TiCl_5(O^iPr)]$. For the NMR measurements, the Quadrupolar Carr-Parcell-Meiboom-Gill MAS (QCPMG-MAS) methodology was selected to enhance the signal by echo train acquisition and decreasing the NMR line width.[37, 38] While $[H_2NMe_2]_2[TiCl_6]$ shows two relatively narrow lines (<1 kHz) corresponding to the ^{49}Ti and ^{47}Ti isotopomers (Fig. 1a), the Ti complex having one alkoxo ligand does not show any NMR signal under similar conditions, likely due to a too large quadrupolar coupling constant (C_Q) associated with a more asymmetric environment (*vide infra*). Fitting the spectrum for $[H_2NMe_2]_2[TiCl_6]$ yields a quadrupolar coupling $C_Q(^{49}Ti)$ of 3.0 MHz, $\delta_{iso}(^{49}Ti)$ = –250 ppm.

On the basis of the narrow lines, this sample was used for the calibration of NMR measurement parameters, which was of highest importance for the spectra of ZN pre-catalysts. We next focused on ZN catalysts – $TiCl_4$@$MgCl_2(THF)_{1.5}$ – treated with BCl_3 in order to remove possible alkoxo ligands and increase our chances to obtain an NMR spectrum with narrower lines (*vide infra*) (see ESI Fig. S2). The $^{47/49}$Ti QCPMG NMR spectrum of the BCl_3-treated sample shows only a broad feature centred at ca. -280 ppm with a number of spinning sidebands (Fig. 1b), whose peak positions and widths are consistent with a surface Ti site in a similar Ti coordination environment as $[H_2NMe_2]_2[TiCl_6]$. The signal can be modeled by a single Ti site with a chemical shift anisotropy (CSA) tensor defined by $\delta_{iso}(^{49}Ti)$ = –170 ppm, skew (κ) = 0.05, and span (Ω) = 332 ppm, and electric field gradient (EFG) tensor described by a $C_Q(^{49}Ti)$ of 9.3 MHz and an asymmetry parameter (η_Q) of 0.65 using both ^{49}Ti and ^{47}Ti isotopes for the simulation. Note that the larger nuclear quadrupolar moment of the ^{47}Ti isotope leads to a very broad line hardly distinguishable from the background. Overall, such NMR signature is consistent with a Ti coordinated solely to Cl ligands in a distorted octahedral environment (*vide infra*). Notably, no $^{47/49}$Ti NMR signal could be obtained on the pristine sample (without prior treatment with BCl_3) consistent with what we observe for the molecular compound and the expected very large C_Q for a site containing both Cl and OR ligands as revealed by ^{13}C MAS NMR (see ESI Fig. S5 for details).

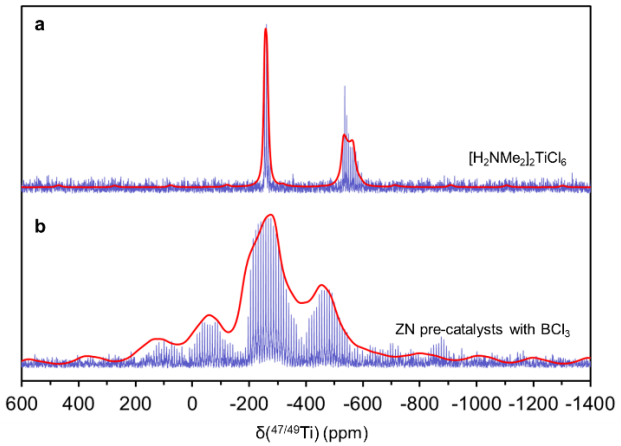

FIGURE 1. $^{47/49}$Ti QCPMG MAS NMR spectra (10 kHz MAS, 21.1 T, 100 K) of (a) $[H_2NMe_2]_2[TiCl_6]$ (512 scans) and (b) ZN pre-catalyst treated with BCl_3 (370'496 scans) as well as the respective modeled line shape (solid red line) for δ_{iso} = -170 ppm and C_Q = 9.3 MHz. Magnitude correction was used for the representation.

TABLE 1. Calculated ^{49}Ti NMR spectroscopic signatures (δ_{iso} / ppm, C_Q / MHz) of model Ti surface species in ZN pre-catalysts

Adsorbate	**Model**					
$TiCl_{4-x}(OR)_x$[a]	$[TiCl_{6-x}(OR)_x]^{2-}$		$TiCl_{4-x}(OR)_x$ @$MgCl_2$-110		$TiCl_{4-x}(OR)_x$ @$MgCl_2$-NR	
	δ_{iso}	C_Q	δ_{iso}	C_Q	δ_{iso}	C_Q
$TiCl_4$	-203	2.1	-64	15.3	-122	11.7
$TiCl_3OR$	-573	37.9	-489	27.5	-511	33.8
$TiCl_2(OR)_2$	-	-	-763	30.4	-760	33.7

[a]x = 0, 1 or 2

In this study, we investigated the contributions that affect the NMR signatures – namely the chemical shift anisotropy and C_Q – of molecular model systems as well as model surface species. For this purpose, we conducted DFT calculations of the NMR parameters[39] – using B3LYP,[40, 41] QZ4P,[42] and the all electron scalar relativistic zeroth-order regular approximation (ZORA)[43] – to explore these contributions. For the purpose of benchmarking the computational protocol, we used a library of molecular compounds with previously reported solution $^{47/49}$Ti NMR isotopic chemical shifts and observed a good agreement between computation and experiment (referenced against benchmark correlation, see ESI for details).[44-46] Building on this DFT protocol, the NMR calculations based on the crystal structures of the molecular compounds $[H_2NMe_2]_2[TiCl_6]$ and $[H_2NMe_2]_2[TiCl_5(O^iPr)]$, confirm a very high sensitivity of the chemical shift and C_Q towards substitution between chlorido and alkoxo ligands. Addition of a single alkoxo ligand is enough to decrease the chemical shift from -203 ppm to -573 ppm, but also to induce a significant increase in the C_Q from 2.1 MHz to 37.9 MHz when compared to the hexachlorido compound, $[H_2NMe_2]_2[TiCl_6]$. Consequently, the lineshape of the Ti-alkoxo species is expected to be significantly broadened compared to the highly symmetric $[H_2NMe_2]_2[TiCl_6]$ species, thus explaining the absence of $^{47/49}$Ti NMR signal for $[H_2NMe_2]_2[TiCl_5(O^iPr)]$ and the related supported untreated ZN pre-catalysts under our measurement conditions.[26, 27]

Next, the ^{49}Ti NMR signatures of model ZN surface sites were investigated (see Table 1), inspecting the effect of directly bound ligands (Cl vs. OR) as well as the $MgCl_2$ morphology. Namely, the difference between the representative crystalline (110)-facet[21, 22, 47-51] ($TiCl_{4-x}(OR)_x$@$MgCl_2$-110) *vs.* an disordered environment around Ti/Mg modeled by a nanoribbon structure ($TiCl_{4-x}(OR)_x$ @$MgCl_2$-NR), was analyzed.[35]

The calculated ^{49}Ti NMR signatures for both groups of model systems (crystalline vs. nanoribbon) show a similar trend in the isotropic chemical shift upon introduction of alkoxo ligands (decreasing 300-500 ppm per alkoxo ligand), consistent with what was observed for the Ti molecular systems and the corresponding V-based ZN pre-catalysts[35] and produced differences within the groups in terms of C_Q. For $TiCl_{4-x}(OR)_x$@$MgCl_2$-110 models, the isotropic chemical shift decreases from –64 ppm for the fully chlorinated titanium to –489 and –763 ppm for the mono- and bis-alkoxo systems, respectively. The introduction of alkoxo ligands is accompanied by a drastic increase in C_Q from 15.3 MHz to 27.5 MHz for mono-alkoxo and to 30.4 MHz – for bis-alkoxo. A similar pattern is obtained for $TiCl_{4-x}(OR)_x$@$MgCl_2$-NR models, whose calculated chemical shifts vary from –122 ppm in the fully chlorinated titanium to –511 and –760 ppm for the mono- and bis-alkoxo systems, respectively. Simultaneously, the C_Q changes from 11.7 MHz to 33.8 MHz and 33.7 MHz. For both models, the chemical shift and C_Q values closest to experimentally observed signatures are consistent with the fully chlorinated Ti species (Fig. 2a).

This result also indicates that it is currently only possible to observe $^{47/49}$Ti NMR signatures when Ti is solely decorated by Cl ligands as in the BCl_3-treated ZN pre-catalyst, because of the associated lower C_Q and thereby narrower lines. On the contrary, the untreated ZN pre-catalysts, that has been shown to contain Ti-alkoxo species by ^{13}C NMR, is expected to contain Ti sites with (extremely) a large C_Q leading to significant second-order quadrupolar line broadening (Fig. 2a), which is currently impossible to observe with the state-of-the-art equipment even at prolonged measurement times.[21]

Now, considering the effect of $MgCl_2$ morphologies on NMR parameters for the fully chlorinated Ti sites, the calculated C_Q and η_Q values are 15.3 MHz and 0.40 vs. 11.7 MHz and 0.40 for $TiCl_4$@$MgCl_2$-110 and $TiCl_4$@$MgCl_2$-NR, respectively, while the amorphous model is in better agreement with the experimental data ($C_{Q,\,exp}$ = 9.3 MHz/0.65) (Fig. 2b and 2d). Most notable is the difference in the $^{47/49}$Ti CSA asymmetric

parameter κ, when comparing the two models of $MgCl_2$ support, as already found for the corresponding ^{51}V NMR signatures in V-based ZN pre-catalysts.[33] While the Ti species on crystalline support displays an axially symmetric CSA tensor (κ = 0.85) consistent with an almost C_{2v} symmetry, the sites on distorted $MgCl_2$ possess a non-axially symmetric κ of 0.04, very close to the experimental parameter and consistent with the distorted Ti geometry (κ_{exp} = 0.05, Fig. 2c). Taken together, the NMR parameters of Ti sites observed for the ZN pre-catalyst treated with BCl_3 are best described by a fully chlorinated hexacoordinated and distorted Ti sites adsorbed on disordered (ca. amorphous) $MgCl_2$ support, as illustrated in Fig. 2d.

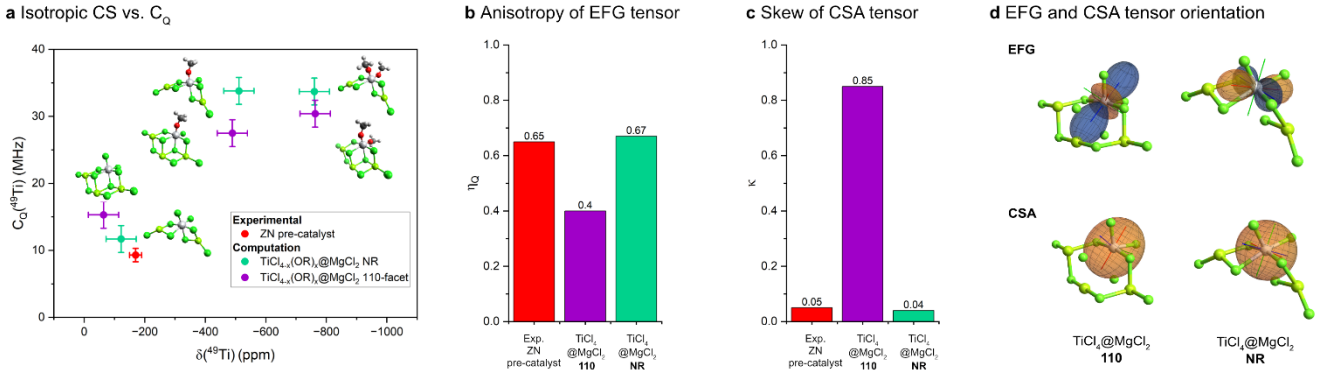

FIGURE 2. (a) Two-dimensional map of calculated ^{49}Ti NMR signatures for the nanoribbon (green points) and (110)-facet model systems (violet points). Experimental value of BCl_3-treated ZN pre-catalysts (red point). The deviations from the computed values were estimated from the benchmark sets for the chemical shift (ca. ±50 ppm) and C_Q (ca. ±2 MHz). (b), (c) Asymmetry and skew parameter of EFG and CSA tensor for fully chlorinated Ti sites on crystalline and distorted $MgCl_2$ supports compared to experimental values. (d) Orientation of respective EFG and CSA tensors.

Considering the sensitivity of the NMR parameters and associated signatures on small differences in coordination environment, induced in particular by the treatment with BCl_3 leading to a substitution of OR by Cl ligands, and its impact on catalytic performances (see ESI Fig. S2), we further examined the origin of the difference of chemical shift. To this end, we inspected the orientation of the chemical shielding tensor (CST) and carried out a Natural Chemical Shielding (NCS)[52-55] analysis of the surface Ti sites in $TiCl_{4-x}(OR)_x$@$MgCl_2$-NR with the goal to rationalize the chemical shift trends observed upon substitution of Cl for OR ligands (detailed analysis of $TiCl_{4-x}(OR)_x$@$MgCl_2$-110-facet in ESI). Notably, the CST orientation strongly depends on the symmetry of these system and the number of terminal Cl/OR ligands. For the fully chlorinated system, $TiCl_4$@$MgCl_2$-NR, the most deshielded component (σ_{11}/δ_{11}) is oriented perpendicular to the plane containing Ti and the two terminal *cis*-Cl ligands (denoted μ_1-Cl), associated with short Ti-Cl bonds (Fig. 3a), with σ_{22} bisecting the μ_1-Cl–Ti–μ_1-Cl angle, and σ_{33} being perpendicular to the other two components. With one terminal alkoxo ligand, as in $TiCl_3OR$@$MgCl_2$-NR, σ_{11} is oriented along the Ti-OR bond, while σ_{22} is oriented perpendicular to the plane containing Ti and the terminal Cl and OR ligands. When both terminal ligands are alkoxo ($TiCl_2(OR)_2$@$MgCl_2$-NR), the CST adopts a similar orientation as in the fully chlorinated system. Notably, the chemical shift across the series of model systems is significantly influenced by the CST component perpendicular to the plane containing Ti and the two terminal μ_1-X (Cl/OR) ligands. The subsequent NCS analysis shows that the chemical shift is mostly driven by the paramagnetic part of the chemical shifts and thereby the nature and the relative energies of high-lying occupied and low-lying unoccupied molecular orbitals, as evidenced by the Ramsey equation (Fig. 3d). The NCS analysis reveals that the chemical shift originates predominantly from the coupling between the σ(Ti-μ_1-X) and π*(Ti-μ_1-X) orbitals, as well as to a smaller extent the corresponding π(Ti-μ_1-X) and σ*(Ti-μ_1-X) orbitals (see Fig. 3b and ESI). The introduction of more electronegative terminal alkoxo ligands results in a larger energy gap between the coupled σ and π* orbitals and consequently to a smaller deshielding as expected from the Ramsey equation[56] (see Fig. 3c):

$$\sigma_{ii,\mathrm{para}} \Leftrightarrow \frac{-\langle\Psi_{\mathrm{occ}}|\hat{L}_i|\Psi_{\mathrm{vac}}\rangle\langle\Psi_{\mathrm{vac}}|\hat{L}_i/r^3|\Psi_{\mathrm{occ}}\rangle}{\Delta E_{\mathrm{vac-occ}}}$$

Overall, we have established a protocol to measure and calculate the $^{47/49}Ti$ NMR spectroscopic signatures for Ti surface sites, focusing here on an industrially relevant ZN pre-catalysts based on $TiCl_4$ adsorbed on $MgCl_2$. We have found that the $^{47/49}Ti$ NMR signatures are highly sensitive to the presence of alkoxo bound to Ti and to the local coordination environment imposed by the morphology of $MgCl_2$ support. Notably, employing QCPMG MAS NMR at 21.1 T and 100 K, a single $^{47/49}Ti$ NMR signature with a chemical shift of -170 ppm, skew of 0.05, C_Q of 9.3 MHz, and asymmetry parameter 0.65 is observed in the ZN pre-catalyst treated with BCl_3, that indicates the presence of a well-defined species with an absence of axial symmetry, best described as a hexacoordinated Ti species adsorbed on a highly flexible ionic disordered $MgCl_2$ (modelled here using the nanoribbon-like structure) with only chlorido ligands. No NMR signal could be observed in the non-BCl_3-treated pre-catalyst sample, consistent with the presence of alkoxo ligands. The observation or non-observation of these species parallels the increased activity observed for BCl_3 treated catalysts,[17] and indicates that having fully chlorinated environment facilitates the formation of the active sites. Observing the structure of this surface species confirms the role of BCl_3 and the support. Detecting the spectroscopic signature of a well-defined structure is particularly noteworthy considering that ZN catalysts are multi-site polymerization catalysts, possibly

pointing out that the complexity of these systems originates from the activation step with the alkyl aluminium reagent rather than the pre-catalyst itself. We are currently exploring the matter in more details by developing methods that would enable observing a broader range of Ti surface sites.

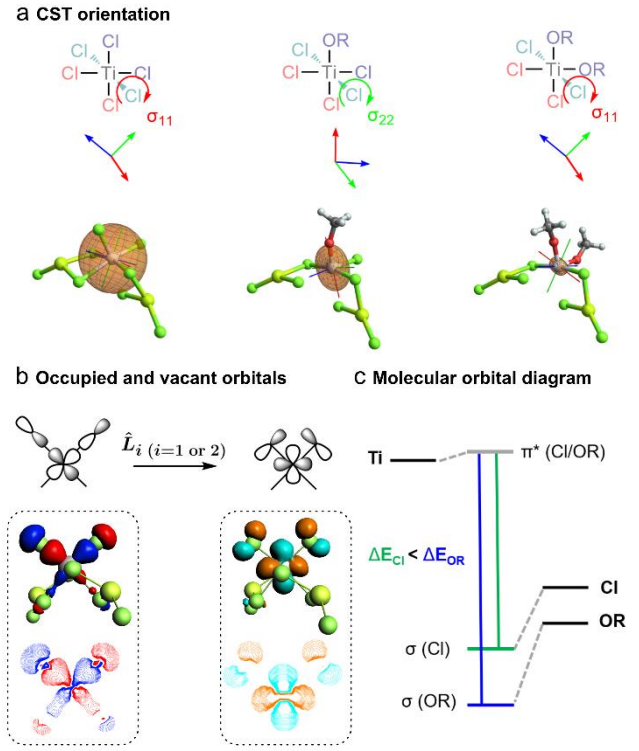

FIGURE 3. (a) Coordination environment of the Ti species with three distinct Cl ligands for $TiCl_4$@$MgCl_2$-NR (terminal: violet, *cis* to both terminal ligands: turquois, *trans* to one terminal ligand: red). Chemical shielding tensor orientation in the $TiCl_{4-x}(OR)_x$@$MgCl_2$-NR model systems (σ_{11} in red, σ_{22} in green and σ_{33} in blue).[57, 58] (b) Rationalisation of the chemical shielding through the visualisation of the corresponding σ - π* Kohn-Sham orbitals obtained from the DFT calculations of the fully chlorinated ($TiCl_4$@$MgCl_2$-NR) surface model, which were selected by reconstruction of the Natural Localized Molecular Orbitals (NLMO) that contribute the most to the deshielding (see ESI). (c) The influence on the MO scheme upon exchanging the terminal ligands rationalizes the large deshielding for the fully chlorinated species compared to alkoxo species.

ASSOCIATED CONTENT

Supporting Information. Synthesis protocols and corresponding solution NMR, single-crystal XRD structures, solid-state NMR measurement parameters and additional spectra, DFT calculation protocol for NMR parameters.

AUTHOR INFORMATION

Corresponding Author

*Alexander Yakimov
yakimov@inorg.chem.ethz.ch

*Christophe Copéret
ccoperet@ethz.ch

‡These authors contributed equally.

ACKNOWLEDGMENT

The authors thank Lyndon Emsley and Laura Piveteau for granting access to the 21.1 T LT NMR spectrometer at EPFL. The Euler supercomputer cluster is gratefully acknowledged for providing computational time. We are grateful to Dr. Matthieu Humbert and Dr. David Gajan (CRMN lab, UMR 5082) for fruitful discussions regarding ^{13}C CP-MAS spectroscopy.

Funding Sources

C.J. Kaul thanks the Swiss National Science Foundation (SNF IZLCZ0_206049) for financial support. Y. K. is grateful to the Swiss National Foundation (SNF) for financial support of this work (grant no. 200020B_192050). This project was partially funded through the ETH+ Project SynthMatLab. F. M. B. thanks the University of Lyon for funding his PhD.

REFERENCES

(1) Ziegler K., H. E., Breil H., Martin H. Das Mülheimer Normaldruck-Polyäthylen-Verfahren. *Angew. Chem.*, **1955**, *67*, 541-547.

(2) Natta, G. Une Nouvelle Classe de Polymeres d'α-Olefines ayant une Régularité de Structure Exceptionnelle. *J. Polym. Sci., Part A: Polym. Chem.*, **1996**, *34*, 321-332.

(3) Natta, G.; Pino, P.; Corradini, P.; Danusso, F.; Mantica, E.; Mazzanti, G.; Moraglio, G. CRYSTALLINE HIGH POLYMERS OF α-OLEFINS. *J. Am. Chem. Soc.*, **1955**, *77*, 1708-1710.

(4) Claverie, J. P.; Schaper, F. Ziegler-Natta catalysis: 50 years after the Nobel Prize. *MRS Bull.*, **2013**, *38*, 213-218.

(5) Kashiwa, N. The discovery and progress of $MgCl_2$-supported $TiCl_4$ catalysts. *J. Polym. Sci., Part A: Polym. Chem.*, **2004**, *42*, 1-8.

(6) Moore, E. P. (Ed.) Polypropylene handbook polymerization, characterization, properties, processing, applications; Hanser Publishers; Hanser Publishers: Munich, Germany. **1996**, 419 p.

(7) Piovano, A.; Signorile, M.; Braglia, L.; Torelli, P.; Martini, A.; Wada, T.; Takasao, G.; Taniike, T.; Groppo, E. Electronic Properties of Ti Sites in Ziegler–Natta Catalysts. *ACS Catal.*, **2021**, *11*, 9949-9961.

(8) Magni, E.; Somorjai, G. A. Preparation of a model Ziegler-Natta catalyst: electron irradiation induced titanium chloride deposition on magnesium chloride thin films grown on gold. *Surf. Sci.*, **1996**, *345*, 1-16.

(9) Mori, H.; Sawada, M.; Higuchi, T.; Hasebe, K.; Otsuka, N.; Terano, M. Direct observation of $MgCl_2$-supported Ziegler catalysts by high resolution transmission electron microscopy. *Macromol, Rapid Commun.*, **1999**, *20*, 245-250.

(10) Fregonese, D.; Glisenti, A.; Mortara, S.; Rizzi, G. A.; Tondello, E.; Bresadola, S. $MgCl_2/TiCl_4/AlEt_3$ catalytic system for olefin polymerisation: a XPS study. *J. Mol. Catal. A: Chem.*, **2002**, *178*, 115-123.

(11) Schmidt, J.; Risse, T.; Hamann, H.; Freund, H. J. Characterization of a model Ziegler–Natta catalyst for ethylene polymerization. *J. Chem. Phys.*, **2002**, *116*, 10861-10868.

(12) Kim, S. H.; Somorjai, G. A. Surface science of single-site heterogeneous olefin polymerization catalysts. *Proc. Natl. Acad. Sci. U.S.A.*, **2006**, *103*, 15289-15294.

(13) Andoni, A.; Chadwick, J. C.; Niemantsverdriet, H. J. W.; Thüne, P. C. A Preparation Method for Well-Defined Crystallites of $MgCl_2$-Supported Ziegler-Natta Catalysts and their Observation by AFM and SEM. *Macromol. Rapid Commun.*, **2007**, *28*, 1466-1471.

(14) Groppo, E.; Seenivasan, K.; Barzan, C. The potential of spectroscopic methods applied to heterogeneous catalysts for olefin polymerization. *Catal. Sci. Technol.*, **2013**, 858-878.

(15) Yakimov, A. V.; Mance, D.; Searles, K.; Copéret, C. A Formulation Protocol with Pyridine to Enable Dynamic Nuclear Polarization Surface-Enhanced NMR Spectroscopy on Reactive Surface Sites: Case Study with Olefin Polymerization and Metathesis Catalysts. *J. Phys. Chem. Lett.*, **2020**, *11*, 3401-3407.

(16) Yakimov, A.; Xu, J.; Searles, K.; Liao, W.-C.; Antinucci, G.; Friederichs, N.; Busico, V.; Copéret, C. DNP-SENS Formulation

Protocols To Study Surface Sites in Ziegler–Natta Catalyst $MgCl_2$ Supports Modified with Internal Donors. *J. Phys. Chem. C*, **2021**, *125*, 15994-16003.

(17) Ashuiev, A.; Humbert, M.; Norsic, S.; Blahut, J.; Gajan, D.; Searles, K.; Klose, D.; Lesage, A.; Pintacuda, G.; Raynaud, J.; et al. Spectroscopic Signature and Structure of the Active Sites in Ziegler–Natta Polymerization Catalysts Revealed by Electron Paramagnetic Resonance. *J. Am. Chem. Soc.*, **2021**, *143*, 9791-9797.

(18) Albizzati, E.; Morini, G.; Giannini, U.; Barino, L.; Scordamaglia, R.; Barbe, C.; Noristi, L. Components and catalysts for the polymerization of olefins. CA2039443A1, **1991**.

(19) Wada, T.; Takasao, G.; Piovano, A.; D'Amore, M.; Thakur, A.; Chammingkwan, P.; Bruzzese, P. C.; Terano, M.; Civalleri, B.; Bordiga, S.; et al. Revisiting the identity of δ-$MgCl_2$: Part I. Structural disorder studied by synchrotron X-ray total scattering. *Journal of Catalysis* **2020**, *385*, 76-86.

(20) Zarupski, J.; Piovano, A.; Signorile, M.; Amodio, A.; Olivi, L.; Hendriksen, C.; Friederichs, N. H.; Groppo, E. Silica-Magnesium-Titanium Ziegler-Natta Catalysts. Part I: Structure of the Pre-Catalyst at a Molecular Level. Part I: Structure of the Pre-Catalyst at a Molecular Level. *J. Catal.*, **2023**, *424*, 236-245.

(21) Blaakmeer, E. S. M.; Antinucci, G.; Correa, A.; Busico, V.; van Eck, E. R. H.; Kentgens, A. P. M. Structural Characterization of Electron Donors in Ziegler–Natta Catalysts. *J. Phys., Chem., C*, **2018**, *122*, 5525-5536.

(22) Blaakmeer, E. S. M.; Antinucci, G.; van Eck, E. R. H.; Kentgens, A. P. M. Probing Interactions between Electron Donors and the Support in $MgCl_2$-Supported Ziegler–Natta Catalysts. *J. Phys. Chem. C*, **2018**, *122*, 17865-17881.

(23) Tijssen, K. C. H.; Blaakmeer, E. S.; Kentgens, A. P. M. Solid-state NMR studies of Ziegler–Natta and metallocene catalysts. *Solid State Nucl. Magn. Reson.*, **2015**, *68-69*, 37-56.

(24) Blaakmeer, E. S.; Antinucci, G.; Busico, V.; van Eck, E. R. H.; Kentgens, A. P. M. Solid-State NMR Investigations of $MgCl_2$ Catalyst Support. *J. Phys. Chem. C*, **2016**, *120*, 6063-6074.

(25) Blaakmeer, E. S.; van Eck, E. R. H.; Kentgens, A. P. M. The coordinative state of aluminium alkyls in Ziegler–Natta catalysts. *Phys. Chem. Chem. Phys.*, **2018**, *20*, 7974-7988.

(26) Grau, E.; Lesage, A.; Norsic, S.; Copéret, C.; Monteil, V.; Sautet, P. Tetrahydrofuran in $TiCl_4$/THF/$MgCl_2$: a Non-Innocent Ligand for Supported Ziegler–Natta Polymerization Catalysts. *ACS Catal.*, **2013**, *3*, 52-56.

(27) D'Anna, V.; Norsic, S.; Gajan, D.; Sanders, K.; Pell, A. J.; Lesage, A.; Monteil, V.; Copéret, C.; Pintacuda, G.; Sautet, P. Structural Characterization of the EtOH–$TiCl_4$–$MgCl_2$ Ziegler–Natta Precatalyst. *J. Phys. Chem. C*, **2016**, *120*, 18075-18087.

(28) Humbert, M.; Norsic, S.; Raynaud, J.; Monteil, V. Activity Enhancement of $MgCl_2$-supported Ziegler-Natta Catalysts by Lewis-acid Pre-treatment for Ethylene Polymerization. *Chin. J. Polym. Sci.*, **2019**, *37*, 1031-1038.

(29) Stone, N. J. Table of nuclear electric quadrupole moments. *At. Data Nucl. Data Tables*, **2016**, *111-112*, 1-28.

(30) Lucier, B. E. G.; Huang, Y. Chapter One - Reviewing $^{47/49}$Ti Solid-State NMR Spectroscopy: From Alloys and Simple Compounds to Catalysts and Porous Materials. In *Annu. Rep. NMR Spectrosc.*, Webb, G. A. Ed.; Vol. 88; Academic Press, **2016**; pp 1-78.

(31) Blaakmeer, E. S.; Wensink, F. J.; van Eck, E. R. H.; de Wijs, G. A.; Kentgens, A. P. M. Preactive Site in Ziegler–Natta Catalysts. *J. Phys. Chem. C*, **2019**, *123*, 14490-14500.

(32) Ohashi, R.; Saito, M.; Fujita, T.; Nakai, T.; Utsumi, H.; Deguchi, K.; Tansho, M.; Shimizu, T. Observation of 47,49Ti NMR Spectra of TiCl4/MgCl2 Catalysts under an Ultrahigh Magnetic Field. *Chem. Lett.*, **2012**, *41*, 1563-1565.

(33) Iijima, T.; Shimizu, T.; Goto, A.; Deguchi, K.; Nakai, T.; Ohashi, R.; Saito, M. 47,49Ti solid-state NMR and DFT study of Ziegler-Natta catalyst: Adsorption of TiCl4 molecule onto the surface of MgCl2. *J. Phys. Chem. Solids*, **2019**, *135*, 109088.

(34) Lätsch, L.; Kaul, C., Yakimov, A. V.,; Müller, I.B., Hassan, A.; Perrone, B., Aghazada, S.; Berkson, Z. J.; De Baerdemaeker, T.; Parvulescu, A.-N.; Seidel, K.; Teles, J. H.; Copéret C. NMR Signatures and Electronic Structure of Ti Sites in Titanosilicalite-1 from Solid-State $^{47/49}$Ti NMR Spectroscopy. **2023**, 145, 15018-15023.

(35) Sabisch S., Kakiuchi Y., Docherty S.R., Yakimov A., Copéret C. Geometry and Local Environment of Surface Sites in Vanadium-Based Ziegler-Natta Catalysts from ^{51}V Solid-State NMR Spectroscopy. *J. Am. Chem. Soc.* **2023**, 145, 25595-25603.

(36) Rannabauer, S.; Schnick, W. Synthese, Kristallstruktur und spektroskopische Charakterisierung von Bis(dimethylammonium)hexachlorotitanat $[Me_2NH_2]_2[TiCl_6]$/ Synthesis, Crystal Structure, and Spectroscopic Characterization of Bis(dimethylammonium) Hexachlorotitanate $[Me_2NH_2]_2[TiCl_6]$. *Z. Naturforsch. B.* **2003**, *58*, 410-414.

(37) Larsen, F.H.; Jakobsen, H.J.; Ellis, P.D.; Nielsen, N.C. QCPMG-MAS NMR of Half-Integer Quadrupolar Nuclei. *J. Magn. Reson.* **1998**, *131*, 144-147.

(38) Iuga, D.; Schäfer, H.; Verhagen, R.; Kentgens, A. P. M. Population and Coherence Transfer Induced by Double Frequency Sweeps in Half-Integer Quadrupolar Spin Systems. *Journal of Magnetic Resonance* **2000**, *147* (2), 192-209.

(39) Becke, A.D. Density-functional thermochemistry. III. The role of exact exchange. *J. Chem. Phys.* **1993**, *98*, 5648-5652.

(40) Becke, A. D. Density-functional thermochemistry. III. The role of exact exchange. *The Journal of Chemical Physics* **1993**, *98* (7), 5648-5652.

(41) Stephens, P.J.; Devlin, F.J.; Chabalowski, C.F.; Frisch, M.J. Ab Initio Calculation of Vibrational Absorption and Circular Dichroism Spectra Using Density Functional Force Fields. *J. Phys. Chem.* **1994**, *98*, 11623-11627.

(42) Van Lenthe, E.; Baerends, E. J. Optimized Slater-type basis sets for the elements 1–118. *J. Comput. Chem.* **2003**, *24*, 1142-1156.

(43) Wolff, S.K.; Ziegler, T.; van Lenthe, E.; Baerends, E.J. Density functional calculations of nuclear magnetic shieldings using the zeroth-order regular approximation (ZORA) for relativistic effects: ZORA nuclear magnetic resonance. *J. Chem. Phys.* **1999**, *110*, 7689-7698.

(44) Hao, N.; Sayer, B.G.; Dénès, G.; Bickley, D.G.; Detellier, C.; McGlinchey, M.J. Titanium-47 and -49 nuclear magnetic resonance spectroscopy: Chemical applications. *J. Magn. Reson.* **1982**, *50*, 50-63.

(45) Berger, S.; Bock, W.; Marth, C. F.; Raguse, B.; Reetz, M. T. $^{47/49}$Ti NMR of some titanium compounds. *Magn. Reson. Chem.* **1990**, *28*, 559-560.

(46) Berger, S.; Bock, W.; Frenking, G.; Jonas, V.; Mueller, F. NMR Data of Methyltitanium Trichloride and Related Organometallic Compounds. A Combined Experimental and Theoretical Study of MenXCl4-n (n = 0-4; X = C, Si, Sn, Pb, Ti). *Journal of the American Chemical Society* **1995**, *117* (13), 3820-3829.

(47) Correa, A.; Credendino, R.; Pater, J.T.M.; Morini, G.; Cavallo, L. Theoretical Investigation of Active Sites at the Corners of $MgCl_2$ Crystallites in Supported Ziegler–Natta Catalysts. *Macromolecules*, **2012**, *45*, 3695-3701.

(48) Breuza, E.; Antinucci, G.; Budzelaar, P.H.M.; Busico, V.; Correa, A.; Ehm, C. $MgCl_2$-Supported Ziegler–Natta Catalysts: a DFT-D "Flexible-Cluster" Approach to Internal Donor Adducts. *J. Phys. Chem. C*, **2018**, *122*, 9046-9053.

(49) D'Amore, M.; Thushara, K.S.; Piovano, A.; Causà, M.; Bordiga, S.; Groppo, E. Surface Investigation and Morphological Analysis of Structurally Disordered $MgCl_2$ and $MgCl_2$/$TiCl_4$ Ziegler–Natta Catalysts. *ACS Catal.*, **2016**, *6*, 5786-5796.

(50) Seth, M.; Margl, P.M.; Ziegler, T.A Density Functional Embedded Cluster Study of Proposed Active Sites in Heterogeneous Ziegler−Natta Catalysts. *Macromolecules*, **2002**, *35*, 7815-7829.

(51) Correa, A.; Piemontesi, F.; Morini, G.; Cavallo, L. Key Elements in the Structure and Function Relationship of the $MgCl_2$/$TiCl_4$/Lewis Base Ziegler−Natta Catalytic System. *Macromolecules*, **2007**, *40*, 9181-9189.

(52) Autschbach, J.; Zheng, S. Analyzing Pt chemical shifts calculated from relativistic density functional theory using localized orbitals: The role of Pt 5d lone pairs. *Magn. Reson. Chem.*, **2008**, *46*, S45-S55.

(53) Widdifield, C.M.; Schurko, R.W. Understanding chemical shielding tensors using group theory, MO analysis, and modern

density-functional theory. *Concepts Magn. Reson., Part A*, **2009**, *34A*, 91-123.

(54) Gordon, C.P.; Lätsch, L.; Copéret, C. Nuclear Magnetic Resonance: A Spectroscopic Probe to Understand the Electronic Structure and Reactivity of Molecules and Materials. *J. Phys. Chem. Lett.*, **2021**, *12*, 2072-2085.

(55) Nater, D.F.; Kaul, C.J.; Lätsch, L.; Tsurugi, H.; Mashima, K.; Copéret, C. Olefin Metathesis Catalysts Generated In Situ from Molybdenum(VI)-Oxo Complexes by Tuning Pendant Ligands. *Chem. Eur. J.*, **2022**, *28*, e202200559.

(56) Ramsey, N.F. Magnetic Shielding of Nuclei in Molecules. *Phys. Rev.*, **1950**, *78*, 699-703.

(57) Zurek, E.; Pickard, C.J.; Autschbach, J. Density Functional Study of the 13C NMR Chemical Shifts in Single-Walled Carbon Nanotubes with Stone−Wales Defects. *J. Phys. Chem. C*, **2008**, *112*, 11744-11750.

(58) Autschbach, J.; Zheng, S.; Schurko, R.W. Analysis of electric field gradient tensors at quadrupolar nuclei in common structural motifs. *Concepts Magn. Reson., Part A*, **2010**, *36A*, 84-126.